JOURNAL OF MATERIALS SCIENCE 31 (1996) 861–866

Use of electron beam-induced current in a SEM for analysis of space solar cells

C. HARDINGHAM
EEV, Waterhouse Lane, Chelmsford, Essex CM1 2QU, UK

Electron beam-induced current (EBIC) measurements have been made on a variety of GaAs and InP single-crystal space solar cells. Plots of the EBIC gain against beam voltage for homoepitaxial GaAs, heteroepitaxial GaAs/Ge and InP solar cells, are presented. Direct correlation between the photovoltaic performance of the cells and the EBIC gain measurements is demonstrated. Quantifiable deterioration of the diffusion lengths, determined by applying Monte Carlo techniques, is evident after irradiation of cells with high-energy protons to simulate the environment in space.

Nomenclature

D	diffusion coefficient
E	electric field
J_{DR}	current density from depletion region
J_n	current density from emitter
J_p	current density from base
k	Boltzmanns constant
L	diffusion length
n	electron density
n_{p0}	equilibrium electron density
p	hole density
q	electronic charge
S	surface recombination velocity
T	temperature
W	depletion region width
x	distance
x_0	surface position
x_J	function depth

Greek symbols

$\alpha(\gamma)$	wavelength dependent absorption coefficient
μ_n	electron mobility
τ_n	electron lifetime
ΦT	incident flux times optical transmission coefficient

1. Introduction

The use of electron beam-induced current (EBIC) techniques in a SEM, to study compound semiconductor solar cells designed for application in space, is reported. As with any other semiconductor device type, the performance of a solar cell is dependent on both the device design and the material properties. Because a solar cell is designed efficiently to collect carriers which are generated by insolation, the device is ideally suited to study by an electron beam-induced current, which also relies on collection of carriers, in this case generated by the primary electron beam in a SEM. Non-destructive EBIC techniques can readily be used to investigate the material properties of working production devices.

The charge collection efficiency (CCE) at any primary beam voltage can be derived from the EBIC gain (collected current/beam current). If the spatial distribution of carrier generation is known, the CCE (or EBIC gain) can be modelled. Adjustment of material parameters used in the model, in particular minority carrier diffusion length, allows a fit of the measured CCE to the model for a variety of beam voltages, and hence evaluation of these material parameters.

2. Solar cells for use in space

Ever since the earliest artificial satellites in the 1950s, photovoltaic cells have been their main source of power. The first solar cells used in space were made from crystalline silicon, which is still the most widely used material. However, although the properties of silicon are well understood, and it is relatively cheap (making for a reliable, cost-effective power source), its optical characteristics are not ideal for this application. Its band gap of 1.1 eV is somewhat lower than the optimum of 1.4–1.5 eV for the AM0 space solar spectrum [1]; that of GaAs is 1.43 eV. Also, unlike GaAs and InP, for instance, silicon has an indirect band gap, leading to a low absorption coefficient: 50–200 μm of active device thickness is required, compared to 5–10 μm for GaAs [2]. The larger volume of active material makes a silicon cell more liable to damage from high-energy particle radiation. Large quantities of high-energy electron and protons are trapped in the earth's magnetosphere, and a further source of protons derives from solar flare activity. The performance degradation which this radiation causes in the solar arrays is a major constraint in the operational life of satellites.

Increasing interest has, therefore, been shown over the last two decades, in the use of alternative materials. In particular, GaAs solar cells, grown either

0022–2461

homoepitaxially, or on a germanium substrate, are now finding widespread application [3], where their higher unit cost is offset by better radiation resistance, and balance of system savings due to their higher beginning of life (BOL) efficiencies.

In particular, because a solar cell is a minority carrier device, high-efficiency cells require high-quality material, in order to minimize loss mechanisms, such as non-radiative recombination. Good minority carrier diffusion lengths are required in the active region near the surface, in order to maximize the collection of photo-generated carriers. Knowledge and control of the material properties are thus crucial to effective manufacture.

EBIC has been used previously to determine diffusion lengths in GaAs and InP solar cells (see, for instance, [4, 5]). However, these studies have all involved EBIC scans across the junction, and thus require a cleaved sample. The techniques are thus not applicable as non-destructive tests on real devices.

3. Solar cell structures

The structure of an infinite melt liquid-phase epitaxy (IMLPE) GaAs solar cell is shown schematically in Fig. 1, and described in detail by Cross *et al.* [6]. It comprises a GaAs homojunction; an optically transparent $Al_xGa_{1-x}As$ window layer on top of the *p*-type emitter acts to reduce the interface recombination velocity of the top face of the emitter layer. A SiN antireflective layer maximizes optical transmission to the active part of the structure. The contacts are fine-grain electroplated gold and silver, made directly on to the highly doped *p*-emitter and with an evaporated Au/Ge/Ni contact layer to the *n*-substrate.

The metal organic chemical vapour deposition (MOCVD) GaAs (Fig. 2) and GaAs/Ge solar cells comprise a similar p–n GaAs homojunction; however, in this case the antireflective coating is TiO_x/Al_2O_3. The *n*-type base layer is grown on a highly doped *n*-type buffer. The buffer layer is grown either on to 300 μm thick ⟨1 0 0⟩ GaAs substrates misoriented a few degrees towards ⟨1 1 1⟩ for the homoepitaxial cells, or on a nucleation layer on a 200 μm Ge substrate, misoriented a few degrees off ⟨1 0 0⟩.

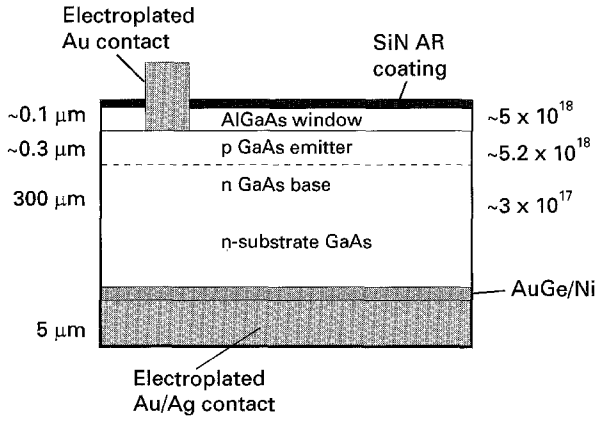

Figure 1 Schematic section through an IMLPE GaAs solar cell structure.

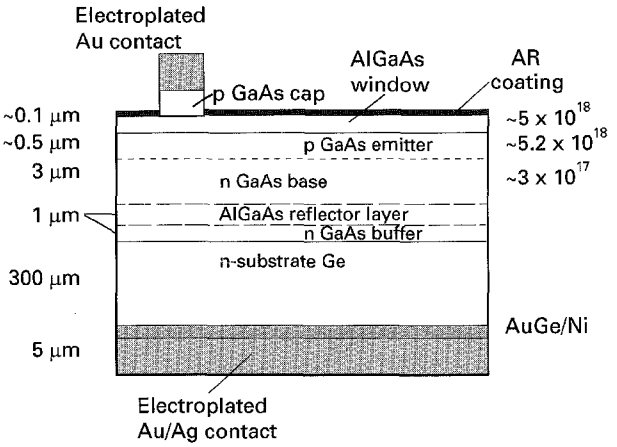

Figure 2 Schematic section through an MOCVD GaAs solar cell structure.

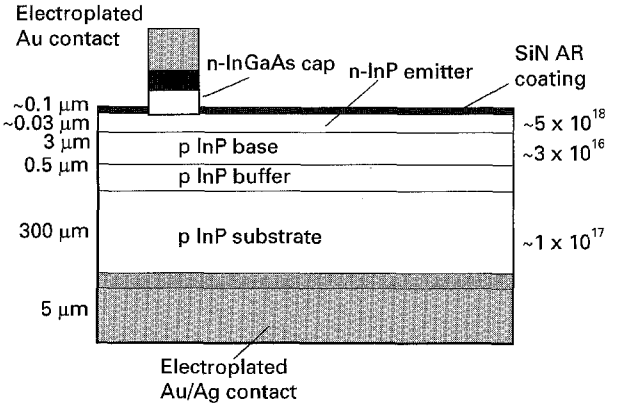

Figure 3 Schematic section through an InP solar cell structure.

The InP structure, shown in Fig. 3, is an n^+–p shallow homojunction: InP does not have a suitable lattice-matched material that can act, as AlGaAs does for GaAs cells, as a window layer to minimize front surface recombination [7]. Instead, a very thin emitter layer is used, so that the least possible light is absorbed in the layer. The actual device design is dominated by the compromise between keeping this layer thin, to minimize surface recombination losses, and keeping the emitter thick enough to carry all the photo-generated electrons, most of which have been swept across the junction, laterally to the metallic grid fingers without significant energy loss (series resistance). Contact is made to the emitter via an n^+ InGaAs cap layer, and to the p substrate directly. The structure and device fabrication are described fully by Hardingham *et al.* [8].

4. Experimental procedure

The solar cells (either 20 mm × 20 mm, or 10 mm × 10 mm) to be studied were mounted whole, using pressure contacts to their front grid and rear face, on an adapted specimen stub, prior to loading into the Jeol 840A microscope. The technique is thus non-destructive, which is useful when working with real operational devices. Electrical connection was made, via a dedicated head-amplifier, to a low-input impedance Matelect current amplifier, from which the

electron beam-induced current, I_{cc}, could be read. Use of the Matelect amplifier to detect photogenerated current in the samples during loading, assisted in ensuring good electrical contact.

The beam current, I_{beam}, was measured by insertion of a Faraday cup into the beam, and measuring the collected current with the Matelect.

The beam accelerating voltage was recorded directly from the selector switch on the control panel. During a set of measurements, the beam current was maintained approximately constant, to within a factor of two, over the range of beam voltages. (At low beam voltages of less than 5 kV, this did not always prove to be possible.) Beam currents were typically 2–4 nA. Measurements were made whilst the beam was rastered, at TV frame rates, over areas typically 500 μm × 300 μm. This was large enough to provide for an average figure for EBIC gain, whilst avoiding the grid fingers (typically at 670 μm spacing).

5. Device modelling

The electron voltaic effect, which forms the basis of EBIC measurements, is closely analogous to the photovoltaic effect, for which the solar cells are designed. In both cases, under low injection conditions (applicable to either moderate electron-beam currents, or 1 Sun optical concentration), the minority carrier concentration within each layer is governed by the continuity equation

$$\frac{1}{q}\frac{dJ_n}{dx} + g(x) - \frac{(n - n_{p0})}{\tau_n} = 0 \qquad (1)$$

where the electron current density is given by

$$J_n = q\mu_n nE + qD_n\frac{dn}{dx}$$

i.e.

$$J_n = q\left(\frac{qD_n}{kT}\right)nE + qD_n\frac{dn}{dx} \qquad (2)$$

5.1. Photovoltaic effect

The carrier generation function, $g(x,\lambda)$, is, in the photovoltaic case, the decaying exponential function due to optical absorption.

Combination of Equations 1 and 2 yields the second-order differential equation in the minority carrier density $n(x)$

$$\frac{1}{\mu_n}\frac{d^2n}{dx^2} + \frac{qE}{kT}\frac{dn}{dx} - \frac{q}{kT}\frac{dE}{dx}n(x) - \frac{[n(x) - n_{p0}]}{L_n^2} - \frac{1}{D_n}g(x) = 0 \qquad (3)$$

This must be solved, to determine the electron carrier density and hence the electron current, subject to two boundary conditions: (i) at the depletion region edge, there is no excess of minority carriers over the equilibrium level; and (ii) at the surface, surface recombination gives

$$\frac{dn(x_0)}{dx} = \frac{S}{D_n}[n(x_0) - n_{p0}] \qquad (4)$$

Where the generation function is due to optical absorption, for simple uniform layers, an analytic solution exists for Equation 3

$$J_n = \left(\frac{q\Phi T\alpha L_n}{(\alpha^2 L_n^2 - 1)}\right)\cdot \left(\left[S_p\frac{L_p}{D_p} + \alpha(\lambda)L_p\right] - e^{-\alpha x_j}\left[S_n\frac{L_n}{D_n}\cosh\frac{x_j}{L_n} + \sinh\frac{x_j}{L_n}\right]\Big/ \left(\frac{S_nL_n}{D_n}\sinh\frac{x_j}{L_n} + \cosh\frac{x_j}{L_n}\right) - \alpha L_n e^{-\alpha x_j}\right) \qquad (5)$$

A corresponding expression holds for the hole current from the n-type region.

Owing to the presence of the built-in field, the residence time of minority carriers in the depletion region is extremely short. Collection from the depletion region may therefore be considered to be 100%

$$J_{DR} = g\Phi Te^{\alpha x_j}[1 - e^{-\alpha W}] \qquad (6)$$

The photogenerated current is the sum of these three components J_n, J_{DR} and J_p.

5.2. Electron voltaic effect

For EBIC, the generation function $g(x,E)$ depends on the beam accelerating voltage, and is more complicated. Approximations, such as assuming uniform generation within a certain sphere of material, may be made, or alternatively, the generation processes may be modelled. This work uses the results from a Monte Carlo simulation of the electrons' trajectories [9] to model the depth distribution of the energy dissipation. Dividing this function by the electron-hole pair formation energy (taken to be three times the material bandgap) yields $g(x)$.

With this form of $g(x)$, the minority carrier equation (Equation 3) is not soluble analytically, and one must resort to numerical methods. For the current work, a fourth-order Runge Kutta method has been used to solve the equation: the starting conditions are iteratively changed using a modified Newton–Raphson method to find a solution which satisfies both boundary conditions.

6. Results and discussion

6.1. IMLPE GaAs solar cells

The variation of EBIC with beam voltage for a typical GaAs solar cell is shown in Fig. 4. The form of the curve is explained as follows: at very low beam voltages (less than about 3 kV), the Grün range of the incident electron beam is very low, so the generation volume only extends through the SiN antireflection layer into the AlGaAs window layer, and not the active part of the device, so no collection is observed. In the range 5–15 kV, the generation volumes lie close to the p–n junction, so almost all charge is generated within a diffusion length of the junction and is therefore collected. Because the charge generated scales linearly with the incident electron energy (or V_{acc}), the

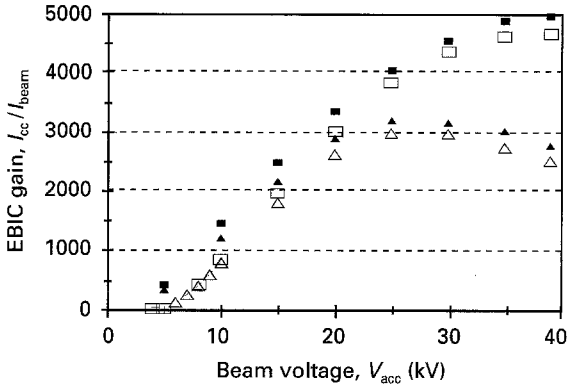

Figure 4 Graph of EBIC gain, I_{cc}/I_{beam}, against beam voltage V_{acc}, for (□) an unirradiated IMLPE cell and (△) a cell irradiated with 10^{12} 1 MeV protons, together with modelled fits to the data, (■, ▲) and triangles, respectively.

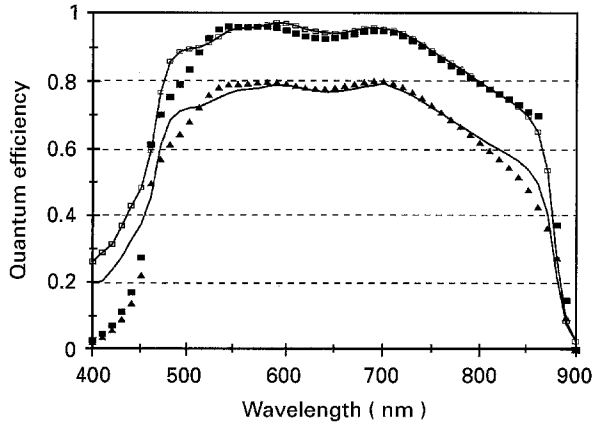

Figure 5 Spectral quantum efficiency of (–□–) an unirradiated IMLPE GaAs solar and (——) a cell irradiated with 10^{12} 1 MeV protons together with modelled fits using parameters for Table I (■, ▲) and triangles respectively.

curve rises linearly in this portion of the curve. At higher beam voltages, however, the gain does not rise so fast, and even starts to tail off, because progressively more of the charge is generated deep within the base, where there is a significant chance of recombination, or even in the buffer or substrate, from which there is very low probability of collection.

Fig. 4 also shows the variation of EBIC gain with beam voltage for an IMLPE GaAs solar cell after irradiation with 10^{12} 1 MeV protons. At low beam voltages the gains are similar. However, at higher beam voltages the gain in the irradiated cell starts to tail off, indicating a higher level of recombination, i.e. shorter diffusion length.

The analogous plot of the variation in quantum efficiency of the cell across the optical spectrum is shown in Fig. 5. The curve has a short wavelength cut-off-due to absorption in the AlGaAs window, an overall rounded shape due to reflection from the surface (the single layer antireflection coating is tuned to 500–600 nm), and a long wavelength turn-off at the GaAs band edge. Superimposed on the general shape are fluctuations with a periodicity of about 100 nm. This is due to the interference-fringing effect of the AlGaAs window, from which one can deduce a window thickness of around 375 nm (on average, over the

TABLE I Parameters use to model QE curves for an unirradiated LPE cell, and a cell irradiated to with 10^{12} 1 MeV protons

		Unirr-adiated	10^{12} protons
AlGaAs thickness (nm)		370	370
Aluminium mole fraction	x	0.89	0.89
Junction depth,	t_J (μm)	0.7	0.7
Front surface recombination,	S_F (cm s^{-1})	1	1
Rear surface recombination,	S_R (cm s^{-1})	1000	1000
Emitter electron diffusion length,	L_n (μm)	2.5	0.95
Base hole diffusion length,	L_p (μm)	2.5	0.7

5 mm × 5 mm region where the measurement was taken).

Fig. 5 indicates a lower quantum efficiency for the irradiated cell, across the whole spectrum. Because, at short wavelengths, the optical absorption of the GaAs is strong, a poor quantum efficiency indicates poor collection from near the surface of the device. Similarly, the long wavelength response, although including a contribution from carriers generated deeper in the device, is still dominated by the emitter response.

Also shown in Fig. 5 are modelled fits to the irradiated and unirradiated cells. The parameters used to provide the fits are listed in Table I below. There is good agreement between the modelled curves and the measured data, apart from in the short wavelength range, 400–500 nm, where the modelled curves indicate very high absorption in the AlGaAs. This may be due to inaccuracies in the AlGaAs data (an empirical fit, due to Jenkins [10], of the experimental data of Aspnes *et al.* [11], was used), or due to some collection from the window layer.

The EBIC response of the cells has been modelled, using the same parameters (apart from AlGaAs thickness). The results are shown in Fig. 4. It can be seen that the model follows the shape of the curves well. The fairly constant offset between the measured and modelled responses is probably due to an underestimate of the window thickness (100 nm was assumed) in the Monte-Carlo calculation of the depth–dose function. The relative significance of this over-estimate decreses at higher beam energies.

Owing to the exponential form of the optical absorption function, modelling of the quantum efficiency plots provides more accurate information about the emitter of the cell, whereas modelling of the EBIC gain provides better information on the base, due to the "mushroom" shape of the generation function resulting from electron beam interactions.

6.2. Proton-irradiated MOCVD GaAs and GaAs/Ge cells

Fig. 6 shows the effect of high-energy proton irradiation (10 MeV in this case), on MOCVD GaAs cells, both homo- and heteroepitaxial. The response of the irradiated cells after low levels of radiation are

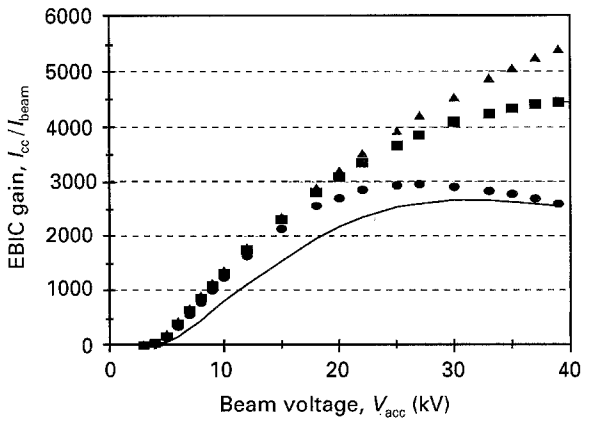

Figure 6 Graph of EBIC gain I_{cc}/I_{beam} against beam voltage, V_{acc}, for MOCVD GaAs cells irradiated with (▲) 10^{10}, (■) 10^{11} and (●) 10^{12} 1 MeV protons and a GaAs/Ge cell irradiated with 10^{12} 1 MeV protons.

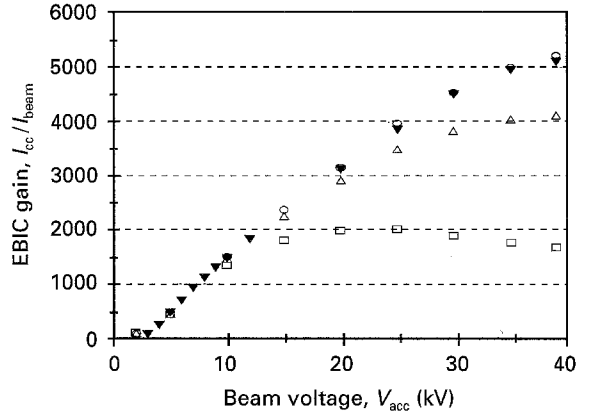

Figure 7 Graph of EBIC gain, I_{cc}/I_{beam}, against beam voltage, V_{acc}, for (▼) an InP cell, together with model results using various values of diffusion length (○) 9 μm, (△) 4 μm and (□) 1 μm.

comparable to the unirradiated IMLPE cells; in fact, it is slightly better, which is indicative that the epitaxial base of the MOCVD cell is better quality than the bulk base of the IMLPE cell. However, after a high radiation dose, the response (particularly at higher beam voltages) is degraded, which is evidence that the lattice is being damaged by the proton bombardment.

The response of a heteroepitaxial GaAs cell after 10^{12} 10 MeV protons is also shown in Fig. 6. In this case, the irradiation affects the cell at much lower beam voltages, which is indicative that the material is being affected higher in the device. (At lower doses, not shown, the response is very similar to the homoepitaxial cell for beam voltages up to 20 kV.) It is possible that the radiation is "unpinning" misfit dislocations which were initially tied to the hetero-interface, thus allowing a higher level of recombination in the emitter.

6.3. InP cells

Fig. 7 shows the variation of EBIC gain with beam voltage, for an InP shallow homojunction cell, together with a modelled response with various values of the base (electron) diffusion length. In this case, a simplified model is used; the effects of (front) surface recombination on the emitter response, and interface recombination at the rear of the base are neglected. The modelling then reduces to a simple calculation of the probability of generated minority carriers diffusing to the junction and being collected. This is justified, because the emitter contributes little to the EBIC response, and the highly doped buffer and substrate are efficient at minimizing the rear interface recombination.

The sensitivity of the response to the diffusion length is clear: the fit demonstrates very good quality material, which is consistent with the > 18% photovoltaic conversion efficiency achieved with this device.

As indicated in Section 5.2, the electron-hole formation energy, E_f, must be known to carry out the modelling described above. For GaAs, the value of 4.2 eV (i.e. $3E_g$) is widely used in the literature, and this value has been used for this work. However, for InP, the value is less well known. In this work 4.0 eV (i.e. $3E_g$) has been used. The excellent fit obtained at low beam voltages, where most generation occurs close to the junction and near unity collection may therefore be expected, provides strong evidence that this value is indeed correct to within ± 10%.

7. Conclusion

Non-destructive EBIC measurements, on plan view III–V space solar cells, have been made. It has been shown how to model the current gain observed, and this modelling has been applied to InP and GaAs solar cells, both as-made and after irradiation with high-energy charged particles. Quantitative information about the degradation in the material quality, after irradiation, has been obtained. Strong evidence for a value of 4.0 eV for the electron-hole formation in InP has been shown.

Acknowledgements

The author acknowledges helpful and stimulating discussions with Professor D.B. Holt, and both the financial support from EEV and assistance, with samples, of Dr T.A. Cross and his co-workers.

References

1. H. J. HOVEL, "Solar Cells", in "Semiconductors and Semimetals", Vol. 11, edited by R. K. Willardson and A. C. Beer (Academic Press, London, 1975) p. 75.
2. C. HARDINGHAM, C. R. HUGGINS, T. CROSS, A. GRAY, K. MULLANEY and C. KITCHEN, in "Proceedings of the 23rd IEEE Photovoltaics Specialists Conference", Kissimmee, edited by S. Bailey (IEEE, New York, 1993) p. 1399.
3. G. C. DATUM and S. A. BILLETS, in "Proceedings of the 22nd IEEE Photovoltaics Specialists Conference", Las Vegas, edited by S. Bailey (IEEE, New York, 1991) p. 1422.
4. M. A. CHUNG, D. L. MEIER, J. R. SZEDON and J. BARTKO, in Proceedings of the 20th IEEE Photovoltaics Specialists Conference", Las Vegas, edited by D. Flood (IEEE, New York, 1988) p. 924.

5. R. HAKIMZADEH and S. BAILEY, in " Proceedings of the XII Space Photovoltaics Research and Technology Conference', Cleveland, OH, edited by N. Fatemi (NASA, Washington, 1992) p. 64.
6. T. A. CROSS, J. BURRAGE, C. HARDINGHAM and A. POTTS, in "Proceedings of the European Space Power Conference", Madrid, edited by J. Landeau (ESA Publications, Noordwijk, Netherlands, 1989) ESA SP294, p. 525.
7. R. JAIN, in "Proceedings of the *23*rd IEEE Photovoltaics Specialists Conference", Loiusville, edited by S. Bailey (IEEE, New York, 1993) p. 7577.
8. C. HARDINGHAM et al., in "Proceedings of the *2*nd European Space Power Conference", Florence, (1991) ESA SP-320, p. 543.
9. E. NAPCHAN, MC-SET Sortware Documentation. (1992).
10. JENKINS J. Appl. Phys **68** (1990) 1848.
11. D. E. ASPNES, S. M. KELSO, R. A. LOGAN and R. BHAT, ibid. **60** (1986) 754.

Received 8 August
and accepted 8 September 1995